Journal of
Polymer & Composites

ISSN: 2321-2810 (Online)
ISSN: 2321-8525 (Print)
Volume 13, Special Issue 6, 2025
DOI (Journal): 10.37591/JoPC

https://journals.stmjournals.com/jopc

Research JoPC

Advanced Polymer Composite Coating for Thermal Performance and EEE Improvement of a Solar Energy Harvesting System

Rahul Sharma[1], Kuwar Mausam[2,*], Kamal Sharma[3]

Abstract

The integration of carbon-based nanomaterials with polymer matrices presents a promising route toward advancing solar energy harvesting technologies. In this study, nanoparticle-blended polymer composite coatings are examined to evaluate the performance of FPSC, utilizing an unconventional collector setup and a multiple-carbon-based nanoparticle-blended paint polymer. Nanomaterial provides a crucial alternative for enhancing their thermal efficiency. The research findings reveal that the deformation of nanomaterials improves the heat efficiency of solar collectors. An experimental analysis is conducted to assess how graphene-based, MWCNT-based, and hybrid graphene-MWCNT selective blended polymer composite coatings influence the performance of an FPSC's absorber plate. Three mixtures were created, varying the concentration of nanoparticles in the carbon-blended black paint polymer. The author performs an experimental work on the flat plate solar collector with nanoparticle blended polymer and compares it with a conventional flat plate collector. Include the following: The possible improvement in the collector efficiency through a hybrid blended polymer composite coating was found to be 34.21% at 1.5 LPM and radiation intensity 800 W/m². The reduction in entropy generation rate is a minimum of 6% by using graphene-blended polymer composite coating at 0.5 LPM and a maximum of 20% by using a hybrid-blended polymer composite coating at 1.5 LPM and a radiation intensity of 800 W/m² as compared to water. The exergy efficiency has been enhanced by 54.71% at 1.5 LPM and a radiation intensity of 800 W/m². This research work highlights the application of carbon-blended black paint polymer blended with the nanomaterials. The research finding indicates that the blending of nanomaterials leads to an improvement in the heat transfer efficiency of the solar collector. This work underscores the role of hybrid polymer–nanomaterial composite coatings in developing next-generation, high-performance solar thermal systems.

Keywords: Composite coating, FPSC, nanomaterial blended polymer, polymer composite characterization, solar intensity, thermal efficiency

***Author for Correspondence**
Kuwar Mausam

[1]Senior Lecturer, Department of Mechanical Engineering, GLA University, Mathura, Uttar Pradesh, India
[2]Associate Professor, Department of Mechanical Engineering, GLA University, Mathura, Uttar Pradesh, India
[3]Professor, Department of Mechanical Engineering, GLA University, Mathura, Uttar Pradesh, India

Received Date: September 02, 2025
Accepted Date: September 12, 2025
Published Date: December 06, 2025

Citation: Rahul Sharma, Kuwar Mausam, Kamal Sharma. Advanced Polymer Composite Coating for Thermal Performance and EEE Improvement of a Solar Energy Harvesting System. Journal of Polymer & Composites. 2025; 13(Special Issue 6): S1197–S1222p.

INTRODUCTION

The primary aim of using advanced polymer composite coatings, particularly those incorporating carbon-based nanomaterials such as carbon nanotubes and graphene blended with paint coatings, in solar energy harvesting systems is to enhance their thermal and optical performance significantly. These coatings are engineered to improve solar absorptivity while minimizing thermal losses, thereby maximizing the conversion of incident solar radiation into usable heat energy. By leveraging the exceptional thermal conductivity, stability, and durability of carbon nanomaterials, the coatings provide superior heat transfer, long-term operational reliability, and resistance to environmental degradation compared to conventional black paints. Ultimately, the use of such advanced coatings aims to increase the efficiency, cost-effectiveness, and sustainability of solar energy harvesting systems, making them more viable for large-scale and long-term applications.

Advanced polymer composite coatings incorporating carbon nanomaterials, such as carbon nanotubes (CNTs) and graphene, demonstrate superior performance compared to conventional commercial coatings. Traditional black paints primarily function as absorptive layers but often suffer from limited thermal conductivity, poor durability under high temperatures, and gradual degradation over time. In contrast, carbon nanomaterial-enhanced coatings offer significantly higher thermal conductivity, improved solar absorptivity, and enhanced resistance to environmental and thermal stresses. Their nanoscale structure not only increases the surface area for better light trapping but also strengthens the coating matrix, resulting in longer service life and stable performance under varying operating conditions. Consequently, these advanced coatings outperform existing commercial alternatives by providing greater energy conversion efficiency, durability, and cost-effectiveness in solar thermal applications.

Carbon nanomaterials, such as carbon nanotubes and graphene, are not biodegradable but can be considered eco-efficient when used in small quantities to enhance material performance, as they reduce the overall material demand and improve energy efficiency in applications like solar collectors. Paint coatings, depending on their formulation, may contain synthetic binders and solvents that pose environmental challenges, though water-based and bio-derived paints are emerging as greener options. Therefore, while not all polymers, nanomaterials, and coatings are inherently eco-friendly or recyclable, research is steadily progressing toward developing sustainable sources and recycling pathways to minimize their environmental impact.

Polymers and polymer-based composites offer unique advantages, including a lightweight structure, thermal stability, ease of processing, and tunable surface properties. Within this domain, the incorporation of carbon-based nanomaterials – particularly carbon nanotubes (CNTs) and graphene – into polymeric matrices has emerged as a novel approach to enhance solar collector performance [1]. Their extraordinary thermal conductivity, optical absorption, and photo-thermal conversion efficiency enable superior heat transfer and retention, making them ideal candidates for modifying absorber surfaces. When blended with black paint polymers, these nanomaterials form hybrid coatings that improve the properties of the collector surface [2].

Solar energy serves as the foundation of life on Earth. The advancement of civilization is closely tied to the availability and use of energy. Conventional energy sources, developed over millions of years through natural and geological processes, are widely used, have mature technology, and ease of access. However, they contribute significantly to environmental pollution through the emission of toxic gases and radiation [3]. In contrast, solar energy is a much cleaner alternative and has emerged as one of the most dependable renewable energy sources. Additionally, solar collectors can capture the portion of solar radiation with the greatest thermal value and convert it into heat, which is transferred to a working fluid circulating through tubes. Among these collectors, FPSCs are the most basic and commonly used due to their simple design, cost-effectiveness, durability, and low maintenance needs [4]. Several factors influence their thermal efficiency, including the position and type of polymers used in the collector plate, glazing material properties, spacing, and diameter of riser tubes, flow rate, radiation intensity, and insulation thickness. The choice of polymers also plays a critical role in optimizing collector performance [5].

Recently, carbon-blended black paint polymer enhanced with nanoparticles has attracted significant research interest for its ability to boost the efficiency of thermal systems. Design optimization of FPSCs is crucial, as it allows for system-specific improvements [6]. Any design modification typically necessitates further adjustments to align with system requirements. The technology behind FPSCs has evolved through consistent research and engineering contributions globally [7].

This summary presents key findings from various researchers: Alvarez et al[8]. used finite element modeling to evaluate solar collectors with corrugated channels. They found that serpentine fluid paths outperform parallel ones in heat transfer. Rey and Zmeureanu [9] demonstrated that combining systems for water heating and space heating reduces building energy demands cost-effectively. Murugan et al[10]. integrated centrally finned twisted inserts and corrugated reflectors, achieving an 11.08% efficiency boost at a twist ratio of Y = 3. Tewari and Dev [11] tested a modified household solar water heater with a non-metallic body and PV module, reporting thermal and exergy gains of 908.9 kWh and 109.56 kWh, respectively. Allouhi et al[12]. an energy and exergy assessment was performed on a forced circulation system integrated with heat pipes, which demonstrated thermal and exergy efficiencies of 33% and 4%, respectively, even under winter conditions. Rodriguez-Hidalgo et al[13]. tested collectors under variable conditions, identifying wind speed as the most influential performance factor. Gunnasegaram et al[14]. showed that double-pass collectors with fins increased efficiency by 9% in certain flow rate and solar intensity ranges. Tanaka [15] studied reflector angles and found that properly inclined reflectors enhanced solar absorption by up to 33%. Cruz-Paragon et al[16]. emphasized testing FPSCs under dynamic conditions using simple design modifications and sensors rather than complex simulations. Mintsa et al[17]. explored the use of polymer instead of copper in collectors and found that a 10 mm air gap significantly improved efficiency. Maldonado et al[18]. reported an average global thermal efficiency of 30.2% for FPSCs based on design and operational parameters. Mansour [19] investigated square mini-channel collector plates, resulting in a 16.1% improvement in heat removal compared to traditional designs. Colangelo et al[20]. demonstrated that using Al_2O_3/water nanofluids reduces sedimentation and enhances thermal conductivity by 5.9% and heat transfer coefficient by 24%. Wang et al[21]. tested a hybrid collector plate (corrugated top, flat bottom) and found it achieved 85.1% efficiency with tilt angle optimization in Guangzhou, China. Visa et al[22]. developed a trapezoidal collector capable of housing a multicolored absorber plate, enhancing versatility and efficiency.

Nikolic and Lukic [23] their findings showed that the new design significantly increased thermal power output, with a peak improvement of 48% compared to conventional collectors. Alvarez et al[24]. explored the impact of a corrugated collector surface through experiments and numerical modeling. Their results showed that the corrugated model achieved the highest energy yield at 86%, outperforming the BBC and Roth-type collectors, which reached 80% and 77.9% respectively. The equivalent collector showed 88% efficiency relative to the BBC type and 44% compared to the Roth type, indicating excellent performance. Hussain and Harrison [25] examined the role of a back-mounted air channel in managing excessive plate temperatures during stagnation (around 170°C). When the channel opened, passive airflow under the hot plate reduced the temperature to 120°C, thereby increasing the collector's durability. Balaji et al[26]. studied the influence of twisted tubes and internal linings as heat transfer enhancers. Unlike earlier approaches, where enhancers were loosely inserted, this method integrated the enhancements into the design. The temperature performance increased by factors of 1.172 and 1.112 for the rod and tube enhancements, respectively, in comparison to the conventional plain tube collector. Facao et al[27]. optimized fluid flow in FPSCs by modifying riser and header configurations. In the Z-shaped design, a more uniform flow distribution was achieved, boosting thermal efficiency [28]. Based on experiments, the author recommended a larger outlet header diameter than the inlet to accommodate the increased fluid volume at higher temperatures. Hassanzadeh et al[29]. introduce the optical and thermal efficiencies reached 64.5% and 50% respectively, at a concentration ratio of 200, achieving a stagnation temperature of 378°C – all without the need for mechanical tracking. Saedodin et al[30]. and Pavlovic et al[31]. compared spiral and conical cavity receivers in solar concentrators, based on both experimental and simulation data, and revealed that conical cavities significantly outperformed spiral ones, achieving a 40.45% increase in thermal efficiency at 200°C and a 42.06% improvement in exergy efficiency.

Testing of the flat plate solar collector design was conducted by ASHRAE guidelines (1993–1997). To ensure consistent testing conditions, experiments were carried out indoors using a solar simulator.

The simulator was equipped with eight halogen lamps, each capable of producing up to 400 watts of light intensity [32]. Control knobs have been used for controlling flow rate and intensity. The experiment was conducted to analyze the thermal performance of an FPSC under controlled environmental conditions. The collector was mounted at a fixed tilt angle corresponding to the local latitude to optimize solar energy absorption [33]. Water served as the working fluid and was continuously circulated through the collector via a pump at a fixed flow rate. Before data collection, the system was allowed to reach a steady-state condition. Temperature sensors were placed at the inlet and outlet of the collector to measure the fluid temperatures [34]. Ambient temperature was also monitored using appropriate meteorological instruments. Data were recorded at regular intervals over several hours during peak sunlight conditions [35]. The collected data were later used to calculate the collector's efficiency and analyze the thermal behavior under varying irradiance and ambient conditions.

Aligned with the research scope of polymer composites and energy-related applications, such nanocomposite coatings contribute to enhanced thermal conductivity, improved surface selectivity, and reduced radiative losses. Furthermore, the structural compatibility and strong interfacial interactions between polymers and nanomaterials ensure stable performance under fluctuating solar radiation and environmental conditions [36]. This synergy not only advances the thermal performance of FPSCs but also significantly improves energy and exergy efficiencies, thereby strengthening their role in renewable energy systems. The experimental investigation was conducted using a standard flat plate solar collector designed to evaluate thermal performance under controlled environmental conditions [37]. The collector features a black-coated absorber plate enclosed within a transparent glass cover to minimize convective and radiative heat losses. A network of copper tubes, bonded to the absorber plate, circulates water as the working fluid [38]. Insulated pipes are used to connect the storage tank to the collector, with a centrifugal pump, which pressurized water flow throughout the system. Temperature changes are tracked using thermocouples positioned at key points like the collector's inlet and outlet, the surrounding air, and the absorber plate's surface [39]. A pyranometer is used to measure solar radiation intensity, while a flow meter records the volumetric flow rate of the working fluid. Data acquisition is handled using a digital temperature logger and a real-time monitoring system [40]. The procedure involves initiating the experiment during peak solar hours (typically between 10:00 AM and 2:00 PM). Initially, baseline readings are recorded before starting the circulation pump. As the fluid passes through the heated absorber plate, its temperature rises, and the corresponding outlet temperature data is logged at regular intervals. The experiment continues until steady-state conditions are achieved. Collected data is then analyzed to calculate useful heat gain, thermal efficiency, and heat loss coefficients [41].

The present work focuses on the thermal performance and EEE improvement of a solar energy harvesting system employing carbon-based nanomaterial blended with black paint polymer. By leveraging the multifunctional capabilities of polymer nanocomposites, the study aims to develop a sustainable, durable, and highly efficient absorber surface coating, bridging the gap between polymer science and renewable energy applications [42].

CHARACTERIZATION OF NANO-BLENDED POLYMER

TGA, XRD, FESEM, and EDAX mapping techniques are used to characterize the nanoparticles, and the TGA results are shown in Figure 1 (a), 3 (a), and 5 (a). From the results, it is clear that the polymer of MWCNT and paint is sustained up to a temperature of 281.07°C, the polymer of graphene and paint is sustained up to a temperature of 283.39°C, and the polymer of Hybrid paint is sustained up to a temperature of 283.86°C. After that, there is degradation of the paint polymer starts. XRD results are illustrated in Figure 1 (b), 3 (b), and 5 (b). MWCNT particles exhibit prominent peaks at $2\theta = 25.7°$, indicating MWCNT presence. Graphene particles exhibit prominent peaks at $2\theta = 26.6°$, indicating their presence, and Hybrid particles exhibit prominent peaks at $2\theta = 26°$ & $26.6°$, indicating their presence.

Journal of Polymer & Composites
Volume 13, Special Issue 6
ISSN: 2321-2810 (Online), ISSN: 2321-8525 (Print)

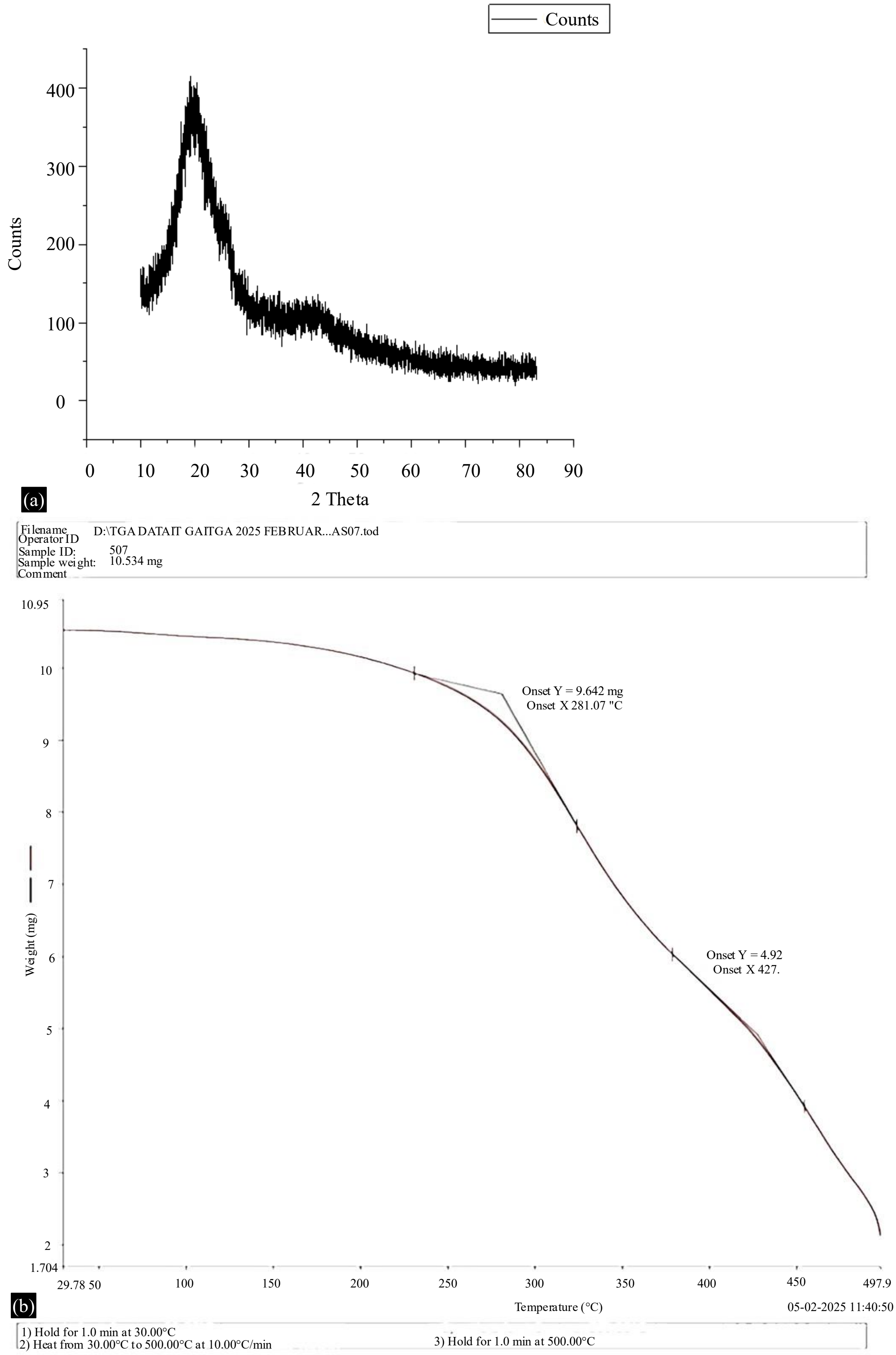

Figure 1. (a) TGA Mapping of MWCNT blended polymer composite coating, (b) XRD mapping of MWCNT blended polymer composite coating.

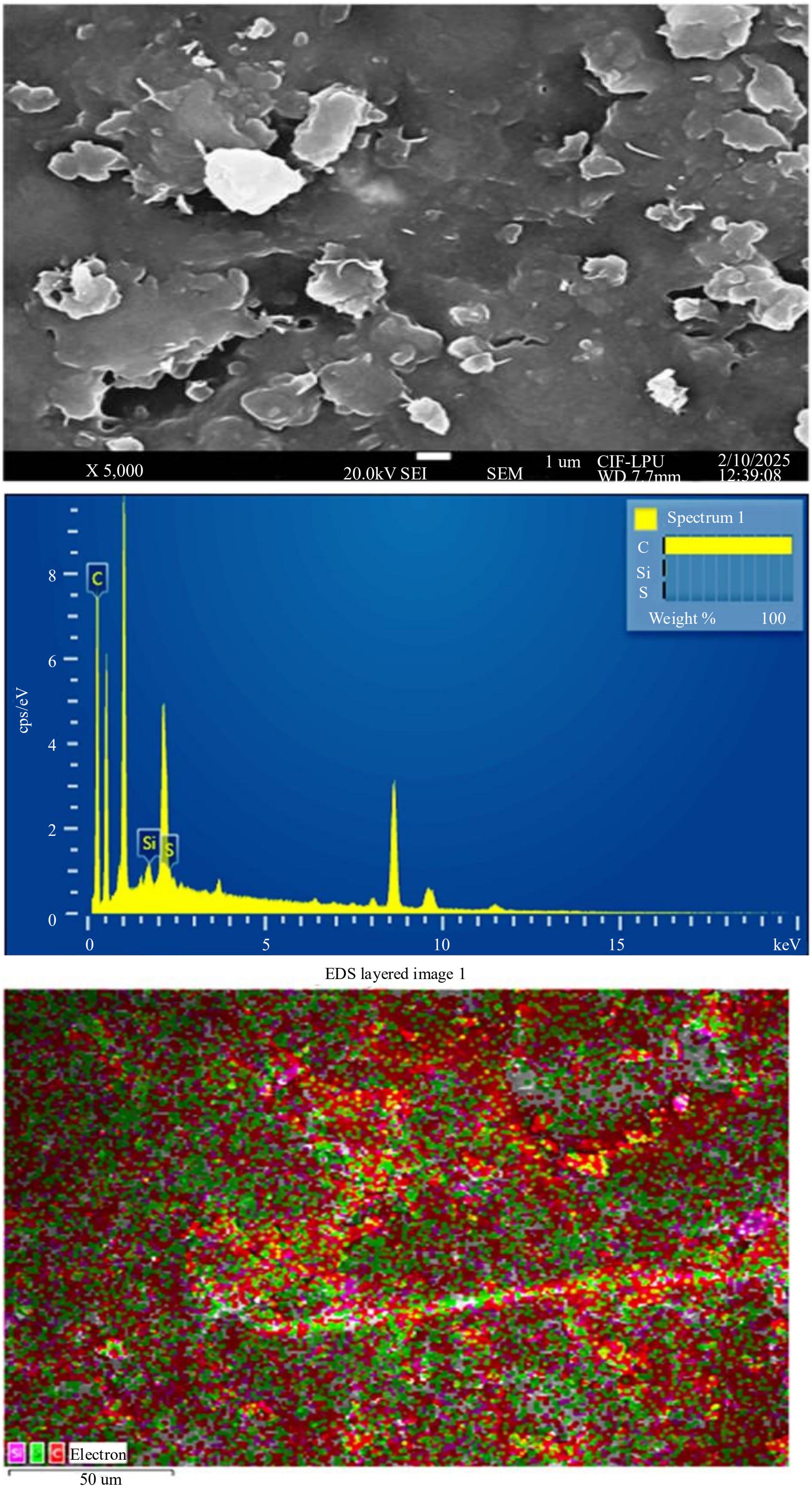

Figure 2. FESEM with EDX mapping of MWCNT blended polymer composite coating.

Journal of Polymer & Composites
Volume 13, Special Issue 6
ISSN: 2321-2810 (Online), ISSN: 2321-8525 (Print)

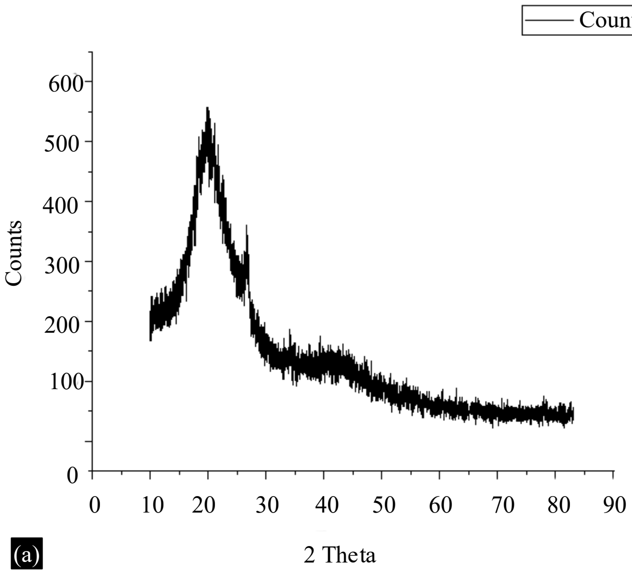

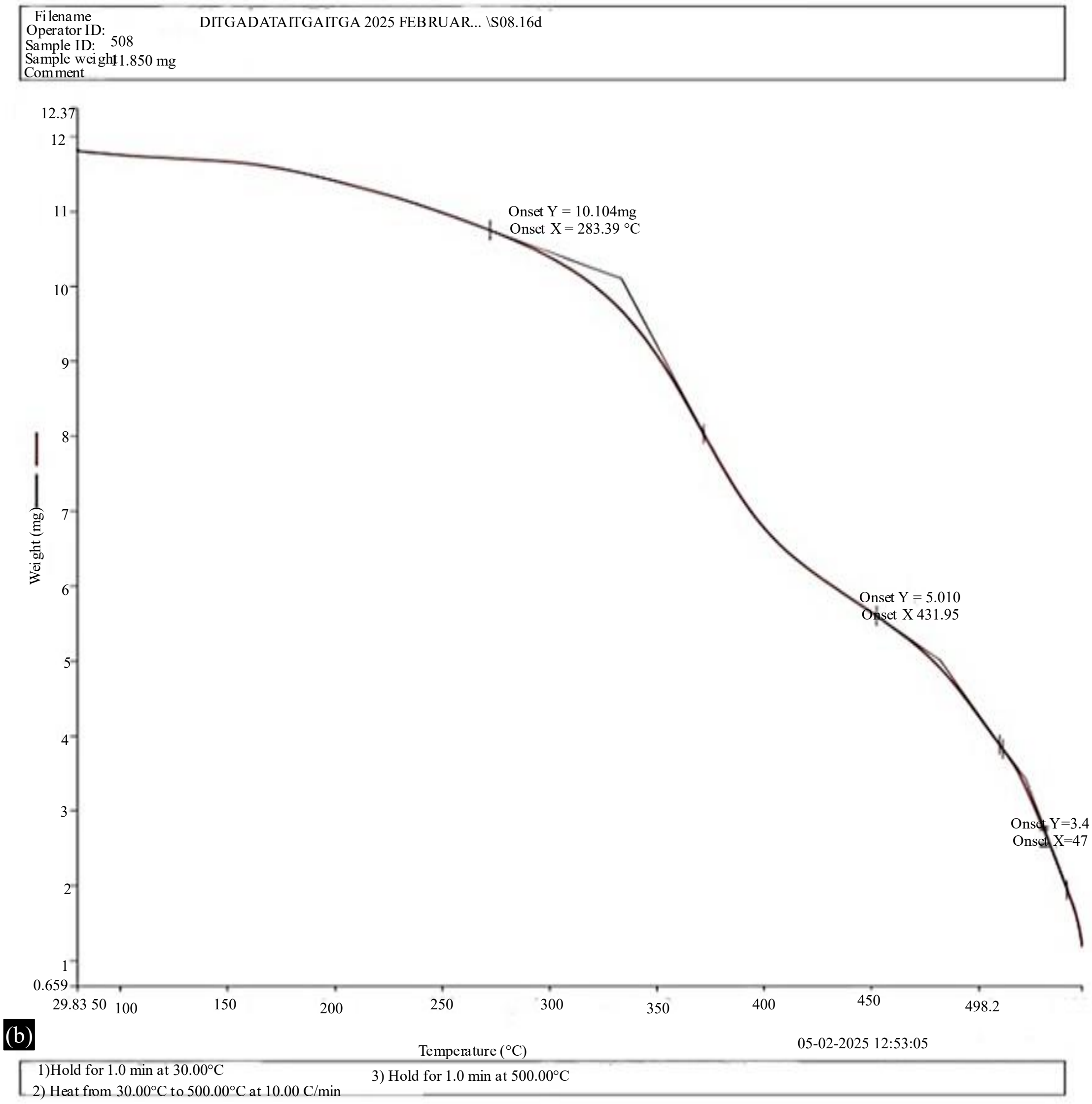

Figure 3. (a) TGA Mapping of graphene blended polymer composite coating, (b) XRD mapping of graphene blended polymer composite coating.

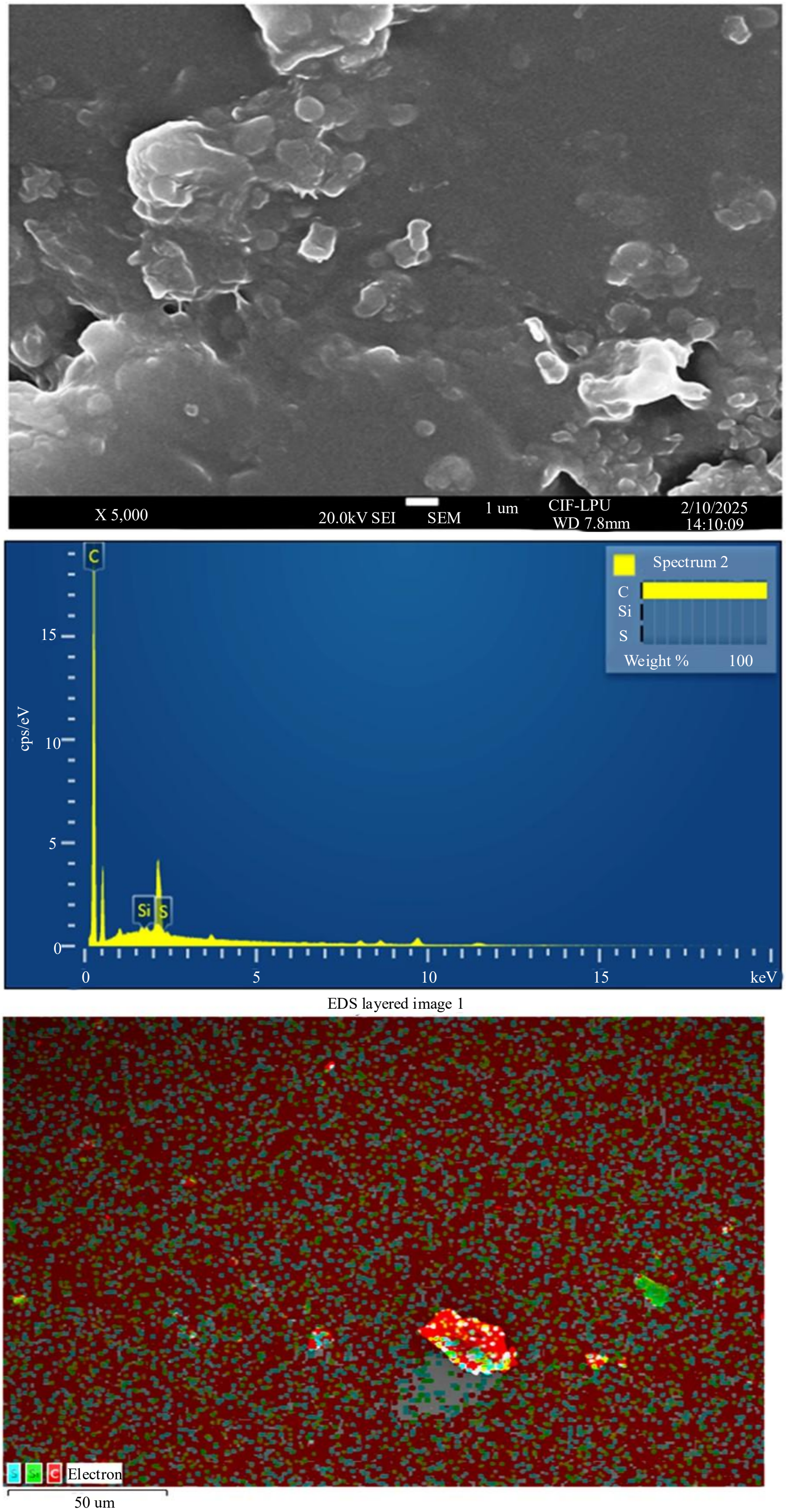

Figure 4. FESEM with EDX mapping of graphene blended polymer composite coating.

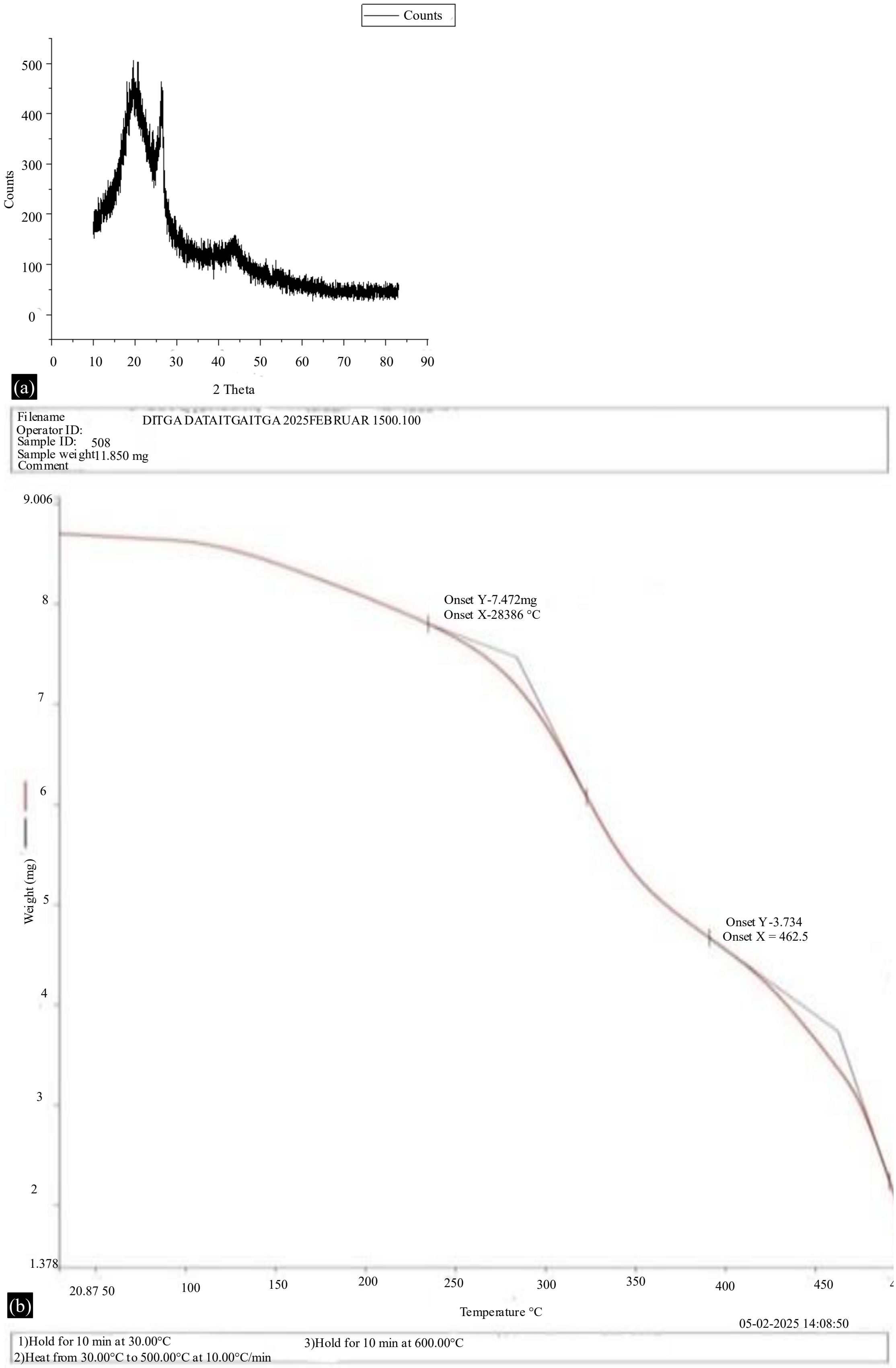

Figure 5. (a) TGA mapping of hybrid blended polymer composite coating, (b) XRD mapping of hybrid blended polymer composite coating.

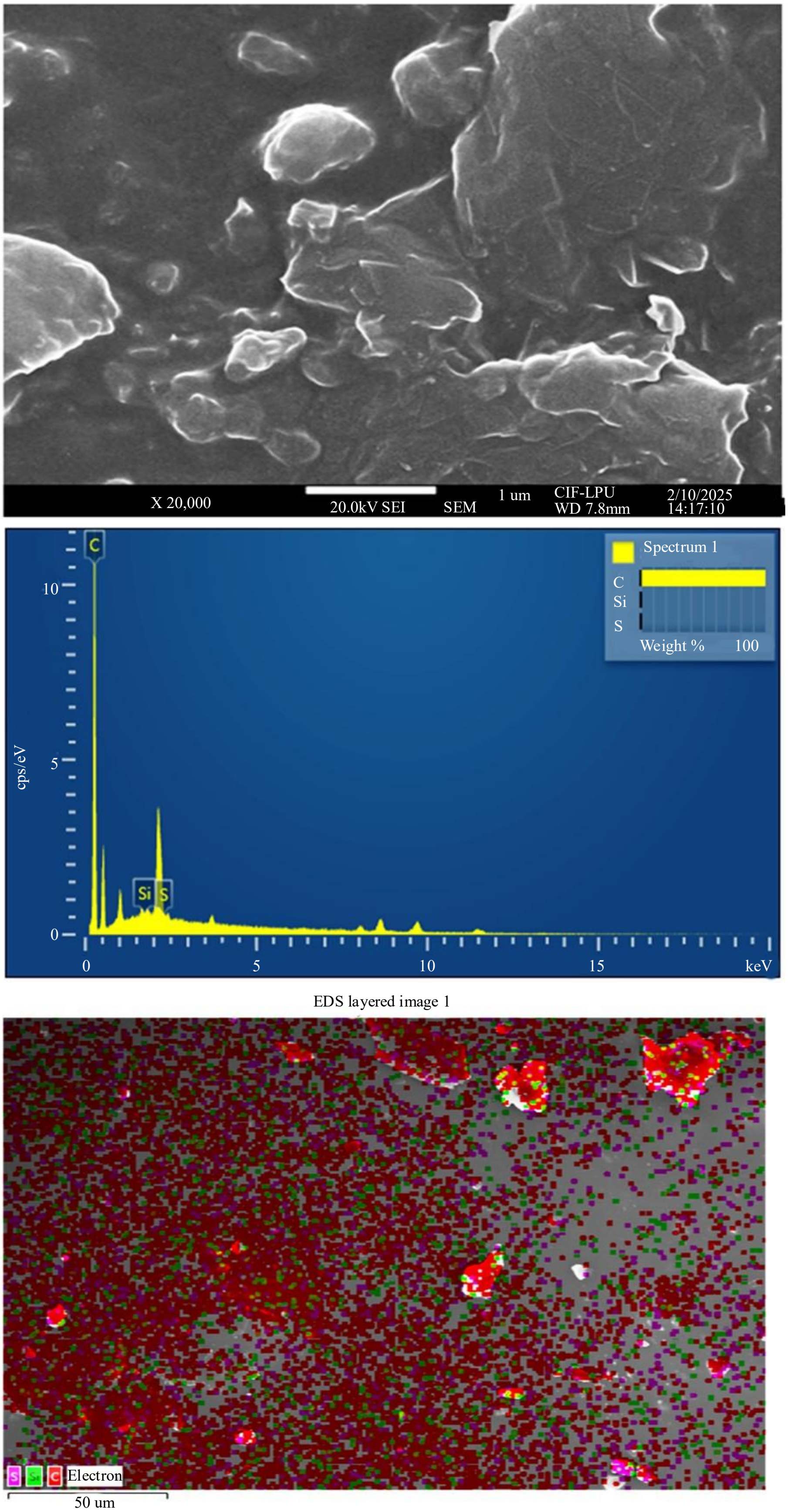

Figure 6. FESEM with EDX mapping of hybrid nano-blended polymer composite coating.

The morphology and particle size were analyzed using FESEM, and EDAX was employed to assess the elemental composition, as shown in Figures 2, 4, and 6. The analysis showed tube-like structures typical of MWCNT, exhibiting an average diameter ranging from 10–15 nm. Aspect ratio falls between 100–5000 or even higher in some cases. Energy-dispersive X-ray spectroscopy (EDAX) further verified the carbon composition (C, Si, and S) of the nanoparticles. Additionally, hexagonal honeycomb lattice structures characteristic of graphene was identified, with particle diameters averaging between 5–10 nm and an aspect ratio of 3000. The EDAX results confirmed the availability of carbon, Si, and S, and the hybrid carbon nanoparticles exhibited tubular and hexagonal honeycomb structures, with diameters averaging between 5 and 15 nm. EDAX results confirmed the predominant presence of carbon within the nanoparticles [43].

PREPARATION OF NANO-BLENDED POLYMER COMPOSITE COATING

Nanoparticle-blended polymer composite coating deposition on a solar collector is a process designed to enhance the efficiency of solar energy absorption, improve thermal conductivity, and reduce reflectivity. The polymer typically consists of nanoparticles engineered to have favorable optical and thermal properties.

Mixing nanoparticles (MWCNT and Graphene) with carbon-blended black paint polymer using a magnetic stirrer involves several key steps to ensure proper dispersion and a homogenous mixture.

Carefully weigh the desired amount of nanoparticle powder based on the target concentration in the final paint polymer mixture. Add the weighed Nanoparticle to a small amount of the chosen compatible solvent in a separate beaker. Use a probe sonicator to sonicate the Nanoparticle-solvent mixture for a specific duration (2–3 hours) at an appropriate power level. Once sonication is complete, put the beaker on the magnetic stirrer and introduce a stir bar. Stir at a moderate speed (500 rpm) for an extended period to further aid dispersion and prevent re-agglomeration. Slowly add the pre-dispersed nanoparticles to the carbon-blended black paint polymer in the main container. The addition should be gradual while stirring to ensure even distribution. Place the container with the carbon-blended black paint polymer and Nanoparticle mixture on the magnetic stirrer. Add a clean stir bar. Adjust the stirring speed of the magnetic stirrer to a level that creates a good vortex without causing excessive splashing or air incorporation. Allow the mixture to stir for a sufficient amount of time to achieve a homogenous dispersion of Nanoparticles throughout the paint. Shown in Figure 7, once a homogenous mixture is achieved, store the Nanoparticle-enhanced carbon-blended black paint polymer in an airtight container to prevent drying or settling.

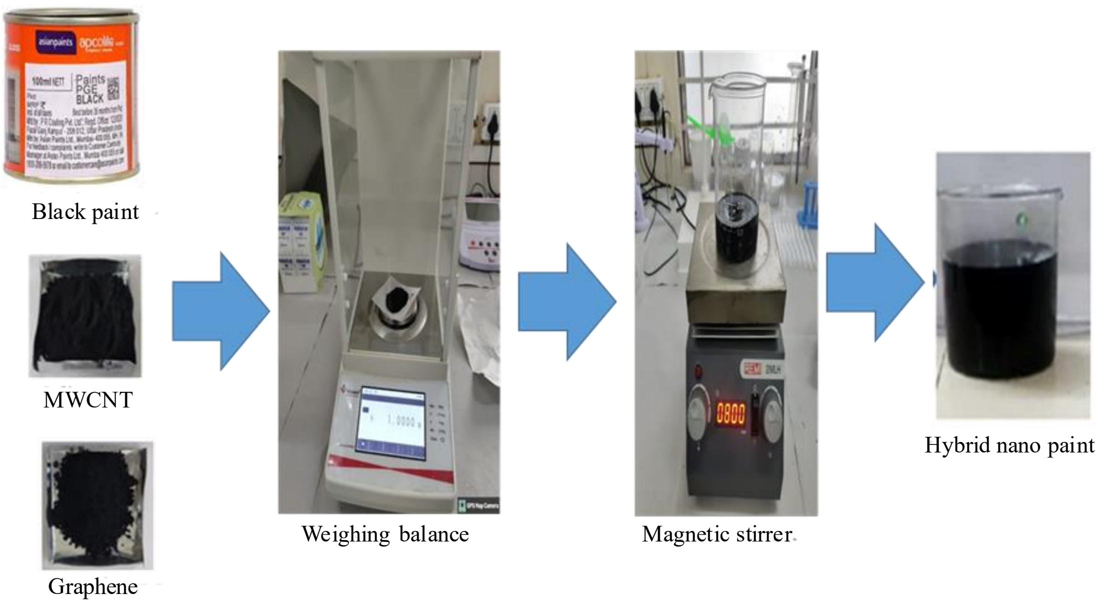

Figure 7. Preparation of a hybrid blended paint polymer composite coating.

The desired properties of the final paint polymer will dictate the concentration of nanoparticles needed. Higher concentrations can lead to enhanced conductivity, mechanical strength, or barrier properties, but might also affect the paint's polymer application characteristics and viscosity. Aerosolized nanoparticle solution is sprayed onto the surface using airbrushes.

EXPERIMENTAL ANALYSIS

Experimental setup

The experimental setup includes the digital interface that displays real-time data, including water flow rate, inlet, outlet, storage tank, ambient air, and plate surface temperatures. Flow rates were measured using a water flow meter equipped with a mini turbine wheel sensor, which provides high precision (1% full-scale deviation) within a range of 0.5–25 liters per minute. For temperature monitoring, Class A sensors were employed, capable of measuring from −200°C to 650°C with an accuracy of ±0.20°C. The intensity of solar radiation was measured with a pyranometer capable of detecting up to 2100 W/m² and having a precision of ±0.10 W/m². The flow diagram of experimental setup is shown in figure 8. The experimental study tested flow rates of 0.5, 0.75, 1.0, 1.25, 1.5, and 1.75 LPM and inclination angles of 45°. The objective was to optimize flat plate collector (FPC) performance in regions with solar radiation levels of 600, 800, and 1020 W/m². Detailed FPC specifications are provided in Table 1.

A Flat Plate Solar Collector (FPSC) consists of several key components. The absorber plate is a flat, thermally conductive surface, typically made from copper, to which fins or tubes are attached for efficient heat transfer. The cover plate is made of toughened glass, chosen for its high transmissivity to solar radiation and strong absorptivity, while also serving to reduce convective heat losses. To reduce heat losses, insulating materials like glass wool and aluminum foil are applied to the rear and side surfaces of the collector. The entire assembly is enclosed within a casing that protects internal components from dust, moisture, and other environmental elements, shown in Figure 10.

Schematic of Working Apparatus

In our experimental setup, a single flow line was used with demineralized (DM) water serving as the conventional working fluid. A rotameter regulated the flow rate, and the water temperature at the inlet was controlled via a heater-chiller system operated by a solenoid valve. Figure 9 illustrates the experimental apparatus employed to evaluate the performance of the improved collector design in comparison to the conventional one. To ensure consistent conditions, testing was primarily conducted indoors using a solar simulator integrated with the apparatus. The simulator can be detached, making it possible to evaluate performance under natural sunlight.

Table 1. The detailed specification of FPC (experimental setup).

Specification	Value	Unit
Collector Dimensions (L × W × H)	53.2 × 43.3 × 8.5	cm³
Absorber Surface Area	0.2	m²
Internal water Tank capacity	50	L
External water tanks Capacity	80	L
Water flow range	0.25 to 25	LPM
Sensor (Thermometers)	200 °C to 600 °C	°C
Radiation	0 to 2000	W/m^2
Glazing Layers	1	–
Tube’s Spacing	20	mm.
Outer Diameter of Collector Tubes	13	Mm
Inner Diameter of Collector Tubes	10	Mm
Tube Center-to-Center Distance	3.5	Mm
Back Insulation Thickness	2.5	mm.
Thermal Conductivity of Back Insulation	0.047	W/m·K

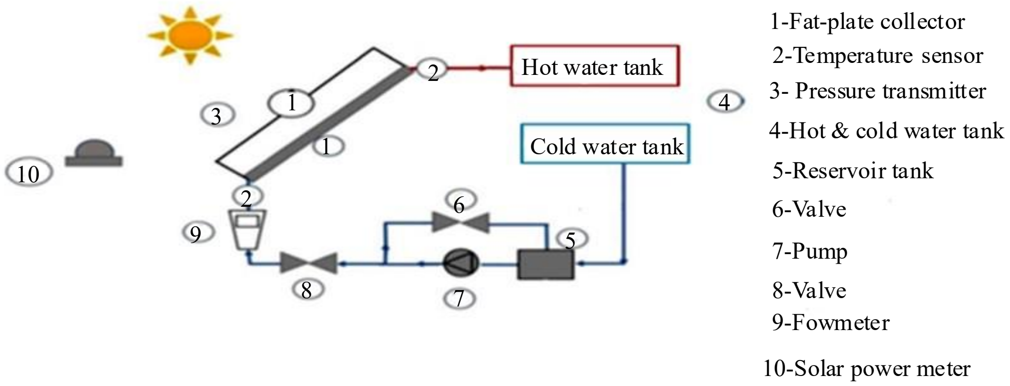

Figure 8. Experimental setup flow diagram.

Figure 11 shows the design of solar collectors, including parallel tube configurations, each with identical collector area, tube diameter, and tube length. Figures 11 provide detailed specifications of the parallel tube collector designs.

MATHEMATICAL FORMULATION EQUATIONS

This section outlines the core mathematical equations used to calculate different efficiencies and performance metrics. The study primarily aims to improve efficiency, with a particular focus on the solar collector's ability to convert incoming sunlight into usable thermal energy – a critical measure of its effectiveness. Key factors influencing this efficiency include glazing transmittance, absorber plate absorptance, and solar radiation intensity. The central goal of the research is to optimize this performance metric. Thermal efficiency, which compares the useful energy output to the total solar energy incident on the collector surface, is the most precise indicator of a collector's performance. Equation (1) [35, 44] can be used to determine the overall heat loss coefficient.

Figure 9. Experimental apparatus.

Figure 10. Parallel tube flat plate collector.

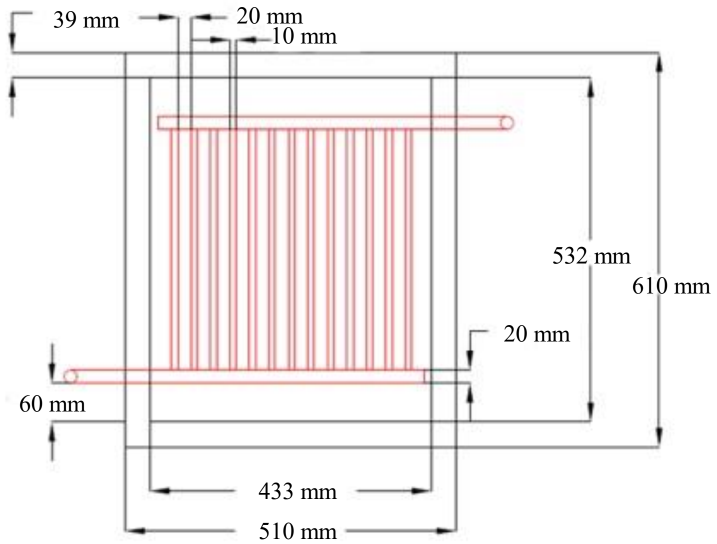

Figure 11. Design Specifications for the Parallel Collector Tube.

The overall heat loss coefficient ( ), calculated using Equation (1) as referenced in [24].

$$U_L = U_t + U_b + U_e \tag{1}$$

The maximum loss coefficient using Klein's correlation formula [45].

$$U_t = \left\{ \frac{\frac{1}{N}}{\frac{C}{T_P}\left[\frac{T_P - T_a}{N+f}\right]^{0.33} + \frac{1}{h_a}} \right\} + \left\{ \frac{\sigma(T_P + T_a)(T_p^{\,2} + T_a^{\,2})}{\varepsilon_P + 0.5N(1-\varepsilon_P) + \frac{2N+f-1}{\varepsilon_g} - N} \right\} \tag{2}$$

$$U_b = \frac{k_b}{x_b} \tag{3}$$

The heat loss coefficient typically falls within the range of 0.4 to 0.7 W/m²·K. s [46]. In a similar manner, the following relationship can be used to determine the heat loss coefficient from the edges of the collector:

$$U_e = U_b\left(\frac{A_e}{A_c}\right) \tag{4}$$

$$F_{HR} = \frac{\dot{m}c_p[T_o - T_i]}{A_{co}[I_{ti}\tau_o\alpha_o - U_{Lc}\cdot(T_i - T_{ab})]} \tag{5}$$

The effective heat gain, (Q_{ug}) is defined through the following equation.

$$Q_{ug} = F_{HR}A_{co}[I_{ti}\tau_o\alpha_o - U_{Lc}\cdot(T_i - T_{ab})] \tag{6}$$

Under steady-state conditions, the thermal efficiency of the flat plate collector, denoted as η_{FP} is defined by the following equation.

$$\eta_{FP} = \frac{\dot{m}c_p[T_o - T_i]}{IA_{co}} \tag{7}$$

Exergy Efficiency (η_{EXfp}) is calculated using the following equation.

$$\eta_{ex} = 1 - \frac{T_a S_{gen}}{\left[1 - \frac{T_a}{T_s}\right]Q_s} \tag{8}$$

Entropy generation (s_{fpgen}) is determined using the equation.

$$\Delta \dot{s}_{gen} = \left(R \ln \frac{p_{out}}{p_{in}} + c_p \ln \frac{T_{in}}{T_{out}} + c_p \frac{T_{out} + T_{in}}{T_a} \right) \Delta \dot{m} + G_c A_c (\tau\alpha) \frac{\Delta T}{T_a^2} + \dot{m} c_p \left(\frac{1}{T_{out}} + \frac{1}{T_{in}} + \frac{2}{T_a} + \frac{(T_{out} + T_{in})}{T_a^2} \right) \Delta T + \dot{m} R \left(\frac{1}{p_{out}} + \frac{1}{p_{in}} \right) \Delta p + A_c (\tau\alpha) \left(\frac{1}{T_s} + \frac{1}{T_a} \right) \Delta G_C \quad (9)$$

EXPERIMENTAL UNCERTAINTIES

The uncertainties encountered during parameter measurements are summarized in Table 2.

$$W = \left[(x_1)^2 + (x_2)^2 + \dots\dots + (x_n)^2 \right]^{1/2} \quad (10)$$

Table 2. The ambiguities in the measurements of the experimental parameters.

Variable	Uncertainty value (%)
Water inlet temperature	±0.18
Water outlet temperature	±0.21
Inlet temperature of hot water	±0.19
Hot Water outlet temperature	±0.22
Mass flow rate	±2.9

FINDINGS AND ANALYSIS

To check the thermal efficiency of FPSC employs water as the working medium. Later, thermal performance evaluation of FPSC has been carried out using graphene-based nano blended polymer composite coating and MWCNT-based nano blended polymer composite coating in FPSC. The operating parameters considered for evaluation of thermal performance of FPSC are mass flow rate varying from 0.5 LPM to 1.75 LPM and solar intensity from 600 W/m², 800 W/m², and 1020 W/m². Experimental tests and performance evaluations were conducted to identify the ideal flow rate and the influence of nanoparticle concentration in paint polymer composite coating on improving solar collector efficiency. Key factors were chosen according to energy balance principles (first law), entropy generation (second law), and exergy efficiency. These variables were examined through experimental testing and compared with simulation results. To minimize environmental fluctuations, the tests were conducted indoors under controlled conditions using an artificial sunlight simulator.

The thermal efficiency of the collector improves with the flow of fluid and the angle of the collector's absorbing surface. The study adhered to ASHRAE guidelines (1993–2003) during experimentation [47]. As illustrated in Figure 12, the collector's instantaneous efficiency correlates with the reduced temperature parameter. The efficiency distribution approximates a straight-line trend, where the slope of the curve increases progressively when the polymer composite coating changes from a conventional carbon-blended black paint polymer composite coating to a hybrid nanoparticle-enhanced carbon-blended black paint polymer composite coating.

The impact of flow rate, inclination angle, and hybrid nanoparticle blended polymer composite coatings (MWCNTs + Graphene + Paint) on the PTC's instantaneous efficiency is shown in Figure 13. The plots for different nanoparticle-blended polymer composite coatings with paint show that efficiency increases in the following order: carbon-blended black paint polymer, graphene, MWCNT, and hybrid nanoparticle-blended polymer.

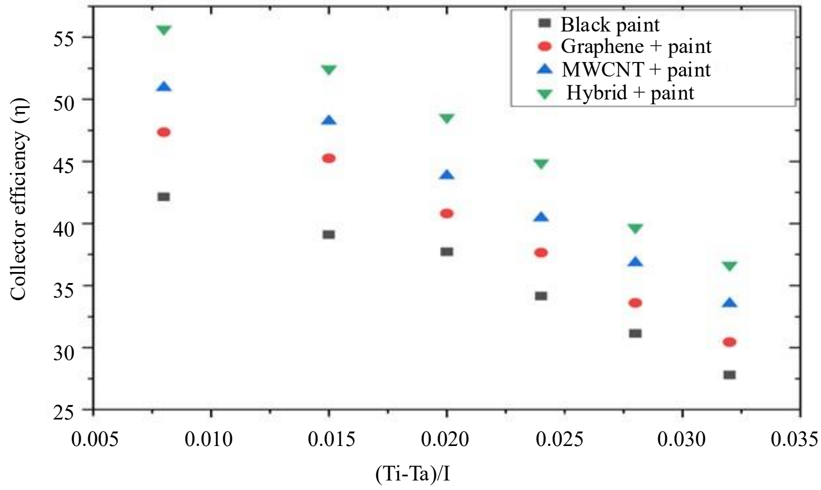

Figure 12. Instantaneous efficiency versus reduced temperature parameter.

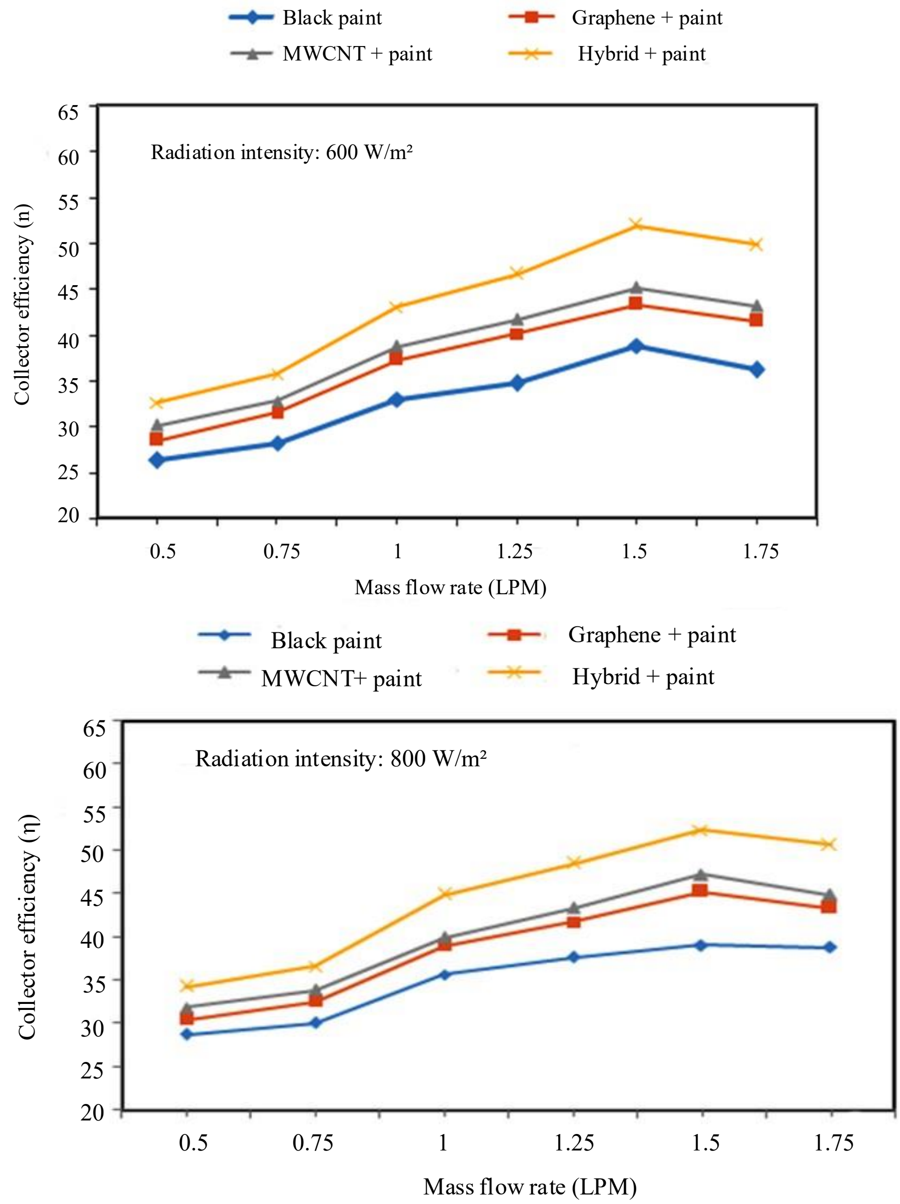

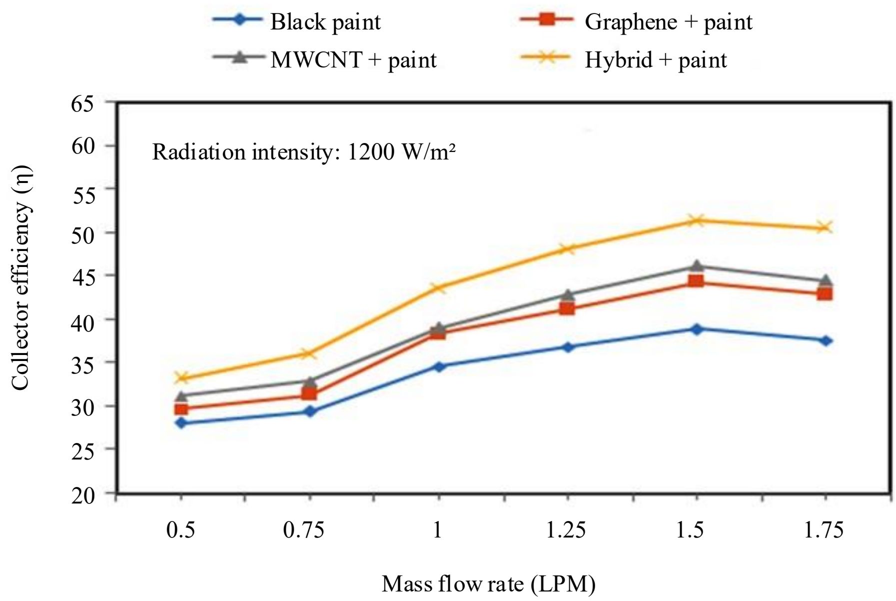

Figure 13. Instantaneous efficiency of the collector for FPC at various flow rates and A 45° inclination angle & radiation 600, 800, and 1020.

As illustrated in Figure 13, the instantaneous efficiency of the solar collector is dependent on the mass flow rate. As the mass flow rate grows, the efficiency enhances, with the most significant improvement observed at 1.5 LPM. However, at higher flow rates, instantaneous efficiency decreases because of the reduced temperature difference between the outlet and inlet fluid. Additionally, pressure drops escalate with increasing flow rates, further lowering thermal efficiency. The experimental findings are examined in three stages. In the first phase, PTC is evaluated for carbon-blended black paint polymer, graphene, MWCNT, and hybrid nano-blended polymer concentrations across flow rates of 0.5, 0.75, 1.0, 1.25, 1.5, and 1.75 LPM at a 45° angle. The most significant enhancement for carbon-blended black paint polymer to graphene, MWCNT, and hybrid nanoparticle blended polymer was 11.72%, 16.36%, and 33.76%, at an inclination angle of 45° with a flow rate of 1.5 LPM and 600 W/m² radiation. The enhancement for carbon-blended black paint polymer to graphene, MWCNT, and hybrid nanoparticle blended polymer was 15.72%, 21.68%, and 34.21%, at an inclination angle of 45° with a flow rate of 1.5 LPM and 800 W/m² radiations.

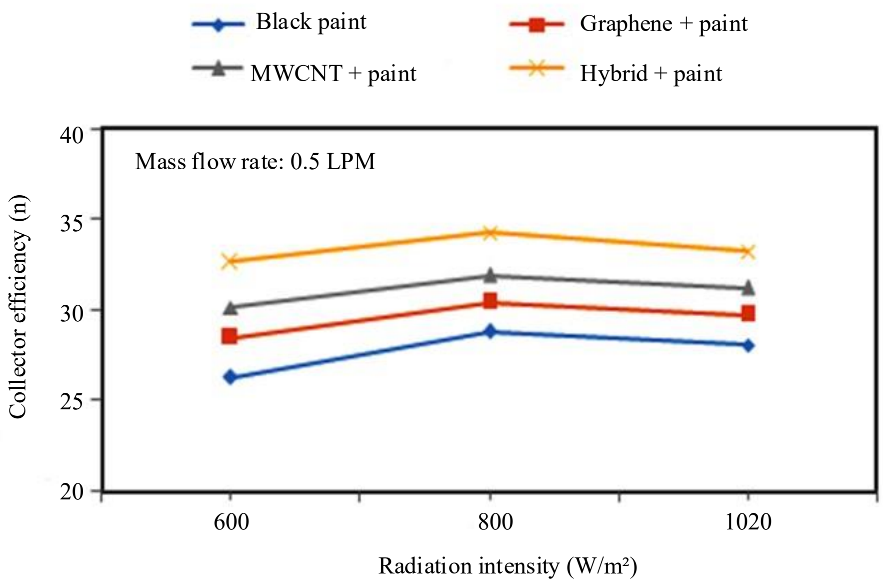

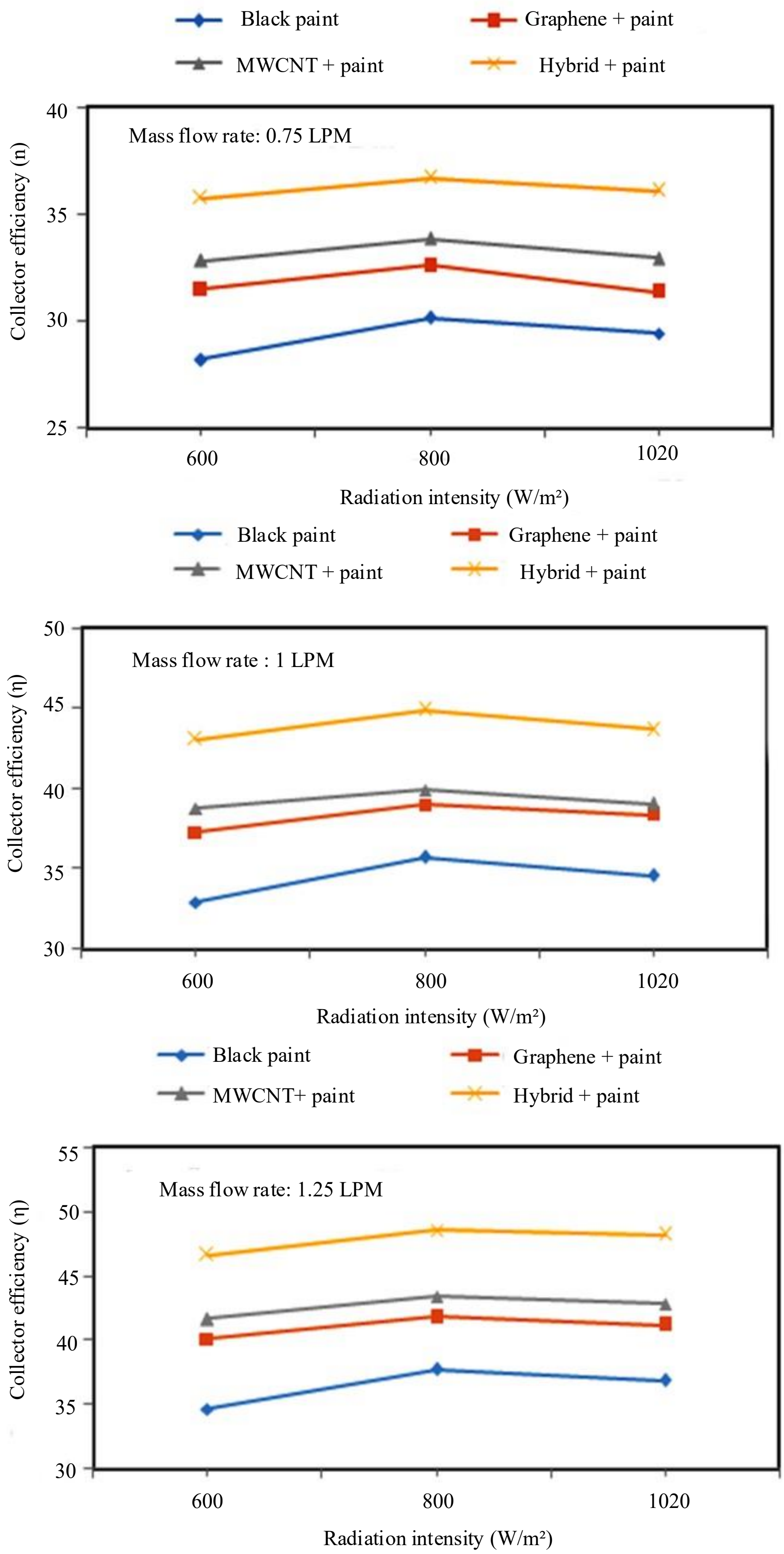
Black paint
Graphene + paint
MWCNT + paint
Hybrid + paint
Mass flow rate: 0.75 LPM
Collector efficiency (η)
40
35
30
25
600
800
1020
Radiation intensity (W/m²)
Black paint
Graphene + paint
MWCNT + paint
Hybrid + paint
Mass flow rate : 1 LPM
Collector efficiency (η)
50
45
40
35
30
600
800
1020
Radiation intensity (W/m²)
Black paint
Graphene + paint
MWCNT+ paint
Hybrid + paint
Mass flow rate: 1.25 LPM
Collector efficiency (η)
55
50
45
40
35
30
600
800
1020
Radiation intensity (W/m²)

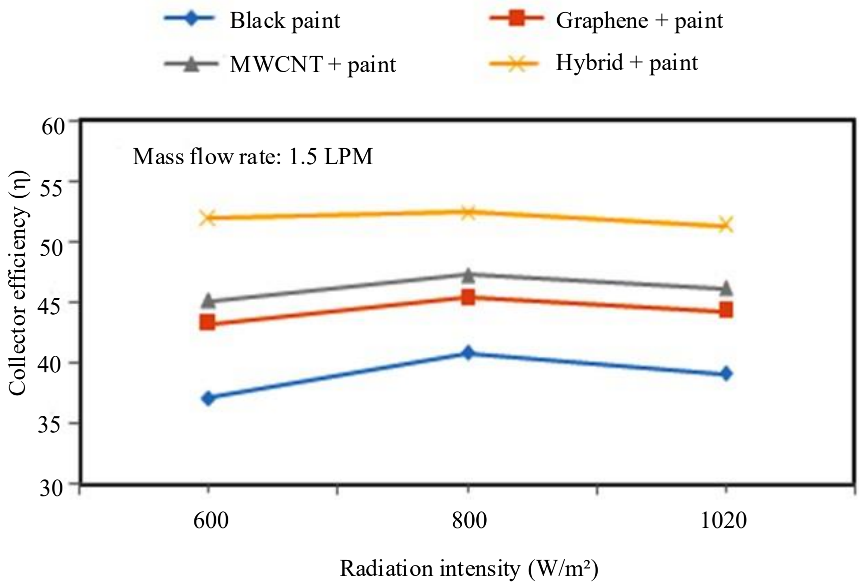

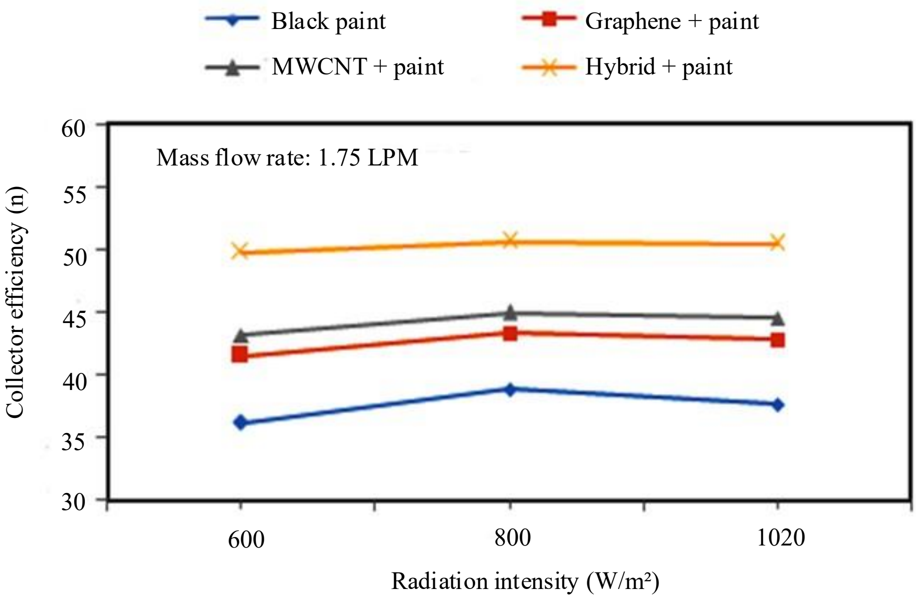

Figure 14. Instantaneous collector efficiency (IE) variation with the radiation intensity at mass flow rate 0.5, 0.75, 1, 1.25, 1.5, and 1.75.

The improvement in carbon-blended black paint polymer to MWCNT, graphene, and hybrid nanoparticle blended polymer was 13.75%, 18.63%, and 31.95%, respectively, at a 45° inclination angle, 1.5 LPM flow rate, and 1020 W/m² radiation. The findings from this experiment indicate that applying a hybrid nanomaterial blended polymer enhances the solar collector's performance. As the flow rate increases, the instantaneous collector efficiency rises to 1.5 LPM, after which it begins to decline.

Figure 14 depicts how the instantaneous efficiency of the PTC varies at a flow rate of 0.5 LPM. The highest efficiency (34.29%) was achieved using a hybrid nanomaterial blended polymer under 800 W/m² solar intensity, showing a 30.38% improvement over the lowest efficiency recorded with water and carbon-blended black paint polymer at 600 W/m². Similarly, at a flow rate of 0.75 LPM, the peak efficiency reached 36.67% for the hybrid nanomaterial blended polymer at 800 W/m², which was 29.94% higher than the minimum efficiency observed with water and carbon-blended black paint polymer under 600 W/m² irradiation.

Figure 14 depicts how the instantaneous efficiency of the PTC varies at a flow rate of 1 LPM. The highest efficiency (44.89%) was achieved using a hybrid nanomaterial blended polymer under 800 W/m² solar intensity, showing a 36.36% improvement over the lowest efficiency recorded with water and carbon-blended black paint polymer at 600 W/m². Similarly, at a flow rate of 1.25 LPM, the peak efficiency reached 48.55% for the hybrid nanomaterial blended polymer at 800 W/m², which was 39.95% higher than the minimum efficiency observed with water and carbon-blended black paint polymer blended polymer under 600 W/m² irradiation.

Figure 14 depicts how the instantaneous efficiency of the PTC varies at a flow rate of 1.5 LPM. The highest efficiency (52.45%) was achieved using a hybrid nanomaterial blended polymer under 800 W/m² solar intensity, showing a 41.37% improvement over the lowest efficiency recorded with water and carbon-blended black paint polymer at 600 W/m². Similarly, at a flow rate of 1.75 LPM, the peak efficiency reached 50.67% for the hybrid nanomaterial blended polymer at 800 W/m², which was 40.08% higher than the minimum efficiency observed with water and carbon-blended black paint polymer under 600 W/m² irradiation.

A peak improvement of 41.37% was recorded with the use of a hybrid nanomaterial blended polymer on the PTC, compared to the carbon-blended black paint polymer, under conditions of 1.5 LPM flow rate, 800 W/m² solar intensity, and a 45° tilt angle.

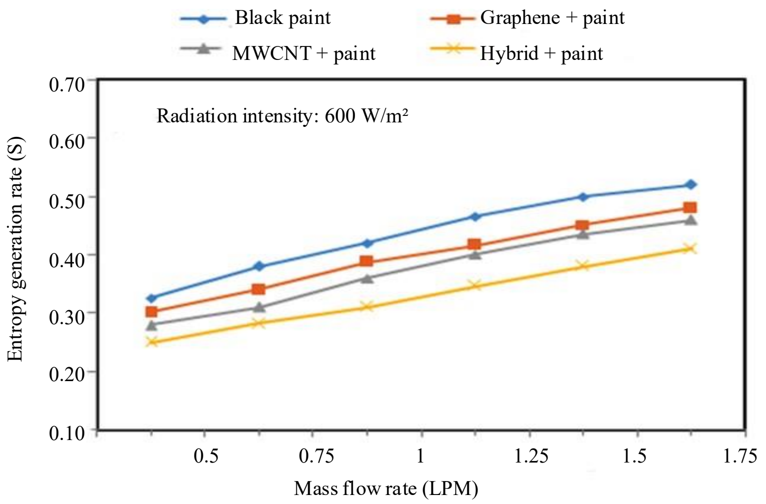

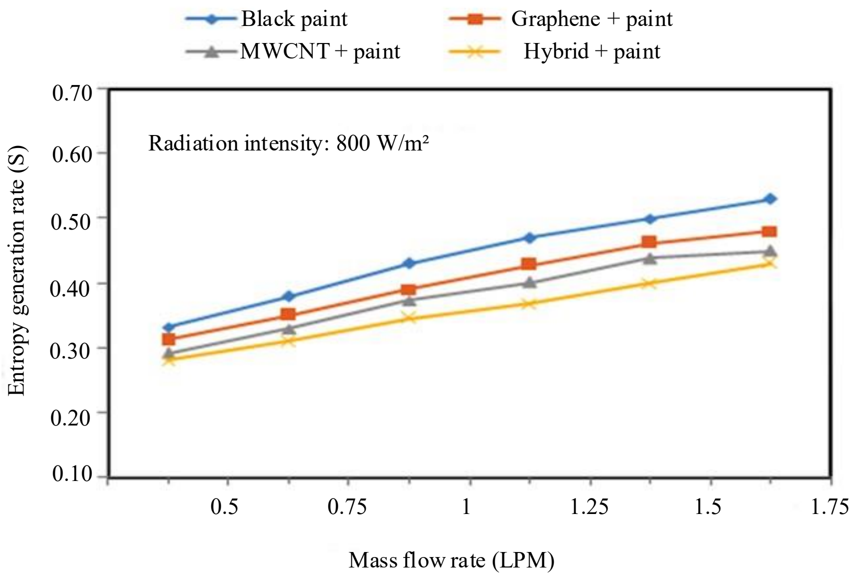

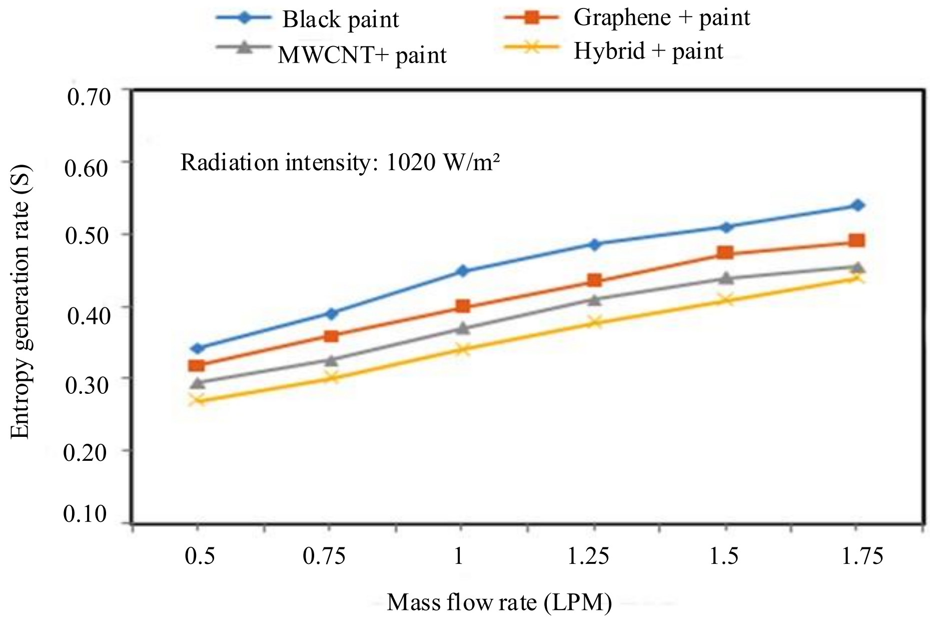

Figure 15. Variation In entropy generation (S) with flow rate (FR) At intensities Of 600, 800, and 1020.

Evaluating entropy generation is necessary for analyzing the exergetic performance of solar thermal systems and plays a notable role in the design and optimization of high-performance thermal setups. A key goal in improving the exergetic efficiency of a solar collector is minimizing entropy production. Enhancing thermal system performance is primarily driven by the need to lower entropy generation. As illustrated in Fig. 15, the rate of entropy generation depends on the mass flow rate as well as the nanomaterial-blended polymer used. It increases with higher mass flow rates. For parabolic trough collectors (PTCs), systems using hybrid nano-blended polymers exhibit lower entropy generation compared to those with conventional carbon-blended black paint polymers. Specifically, a 20% decrease in entropy production is achieved with hybrid nano-blended polymers at a flow rate of 1.5 LPM and solar radiation intensity of 800 W/m². This is attributed to the superior radiation absorption and heat transfer capabilities of hybrid nanoparticles.

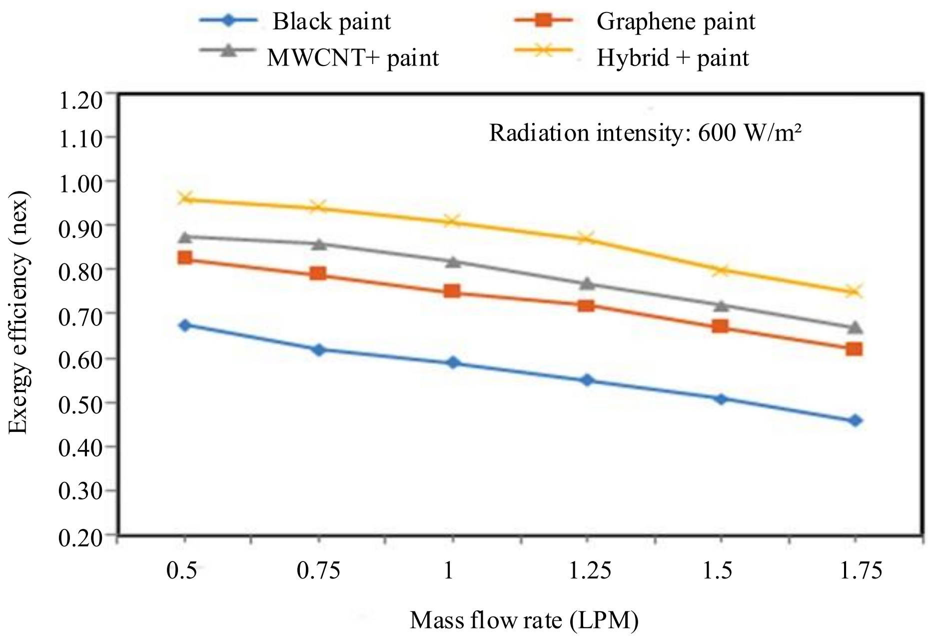

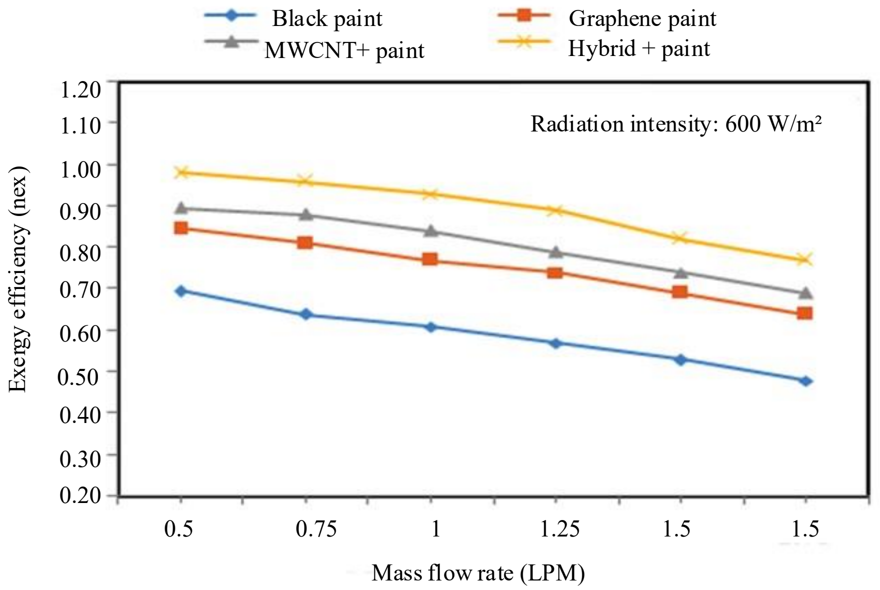

Figure 16. Exergy efficiency (hex) variation with the interaction of flow rate (FR) at intensities (I) 600, 800, and 1020.

Entropy and exergy are interconnected in a mutually beneficial way, though inversely related. Exergy indicates how effectively a thermal system converts available energy into usable work. As shown in Figure 16, exergy efficiency tends to decrease as the mass flow rate increases, but improves with the use of hybrid nanomaterial-coated water.

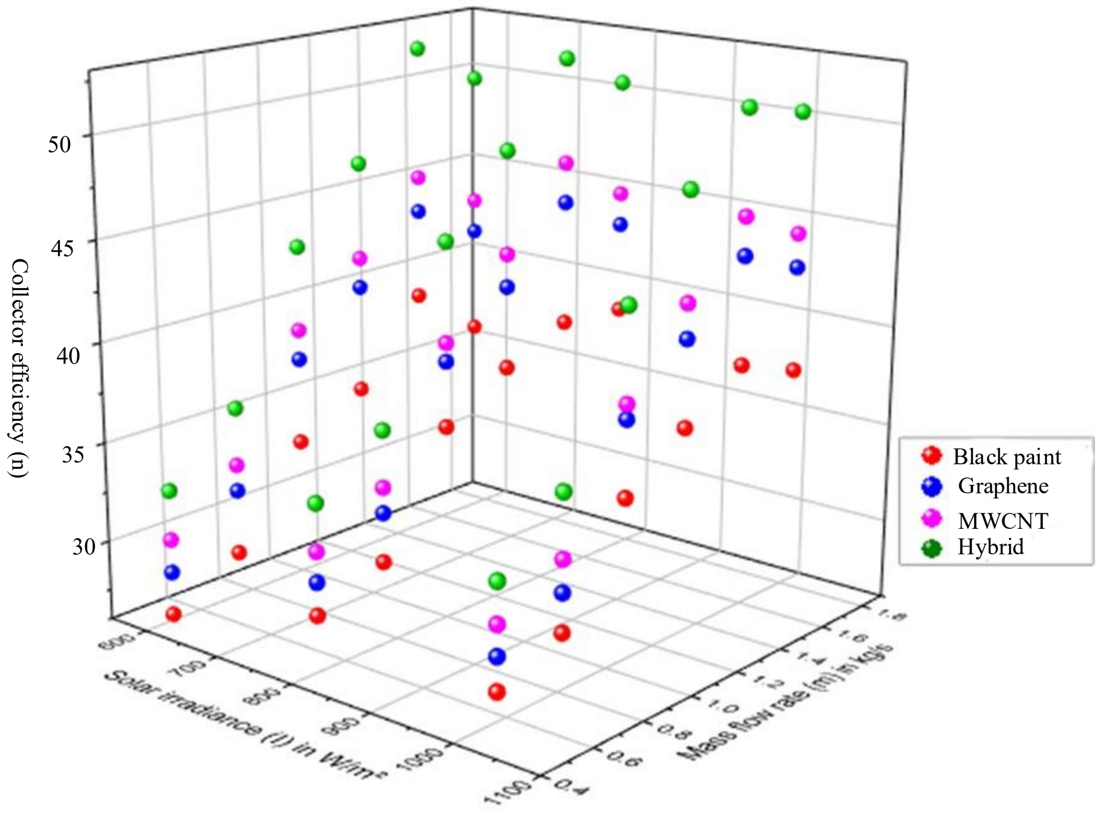

Figure 17. Comparison of thermal efficiency for solar intensity and mass flow rate at different nanomaterial blended polymer composite coatings.

This inverse relationship occurs because higher flow rates generate more entropy, reducing exergy efficiency. A peak exergy efficiency improvement of 54.71% was observed in the PTC system using hybrid nanoparticle blended polymers at a flow rate of 1.5 LPM under 800 W/m² solar radiation.

CONCLUSION

In the above study, the effect of radiation intensity from 600–1020 W/m²K and the effect on the thermal efficiency of solar collectors due to the collector polymer composite coatings of MWCNT and paint, graphene, and paint, and MWCNT and graphene and paint has been studied. The correlation for the thermal efficiency of graphene and MWCNT mix paint polymer composite coating has been developed in terms of operating parameters, i.e., temperature and mass flow rate. Based on the enhancement in thermal efficiency by MWCNT and graphene, the prepared nano-blended polymer composite coating has been used to enhance the thermal performance of FPSC. The notable improvement in the thermal performance for all MWCNT and paint, graphene, and paint, and MWCNT and graphene and paint samples has been reported for temperature, radiation intensity, and mass flow rate, and hence, all three polymer composite coatings can be used as a collector blended polymer composite coating in several thermal appliances.

The thermal efficiency of MWCNT and paint, graphene, and paint, and MWCNT and graphene blended paint polymer composite coating enhances gradually with mass flow rate from 0.5 LPM to 1.5 LPM, and further on increasing the mass flow rate from 1.5–1.75, TC starts decreasing due to the fast flow rate of water and less absorbability of sun radiation. The highest improvement in thermal conductivity was observed under specific conditions of 1.5 liters per minute flow rate, a 45° inclination, and a power density of 800 W/m²; a hybrid nanoparticle blended polymer composite coating improved thermal efficiency by 34.21% compared to a traditional carbon-blended black paint polymer composite coating. For all mass flow rates between 0.5 LPM to 1.5 LPM, the thermal efficiency of MWCNT and paint, graphene, and paint, and MWCNT and graphene and paint increases progressively with radiation intensity and is found to be at its maximum at 800 W/m²K. The maximum enhancement in the collector efficiency through hybrid blended polymer composite coating was found to be 34.21% at 1.5 LPM and radiation intensity of 800 W/m²K.

The correlation has been developed for the thermal efficiency of all three nano-blended polymer composite coatings in terms of temperature and mass flow rate. A comparison between the experimental and predicted results shows a deviation of ±2%, which falls within the acceptable range for all tested mass flow rates (0.5–1.5 LPM) and radiation intensities (600–1020 W/m²). All three nano-blended polymer composite coatings have been used as a collector polymer composite coating in FPSC. The thermal analysis shows that all three nano-blended polymer composite coatings enhance the thermal performance when used as a collector polymer composite coating in FPSC.

The reduction in entropy generation rate is a minimum of 6% by using graphene-blended polymer at 0.5 LPM and a maximum of 20% by using hybrid-blended polymer at 1.5 LPM and a radiation intensity of 800 W/m²K as compared to water. The exergy efficiency has been enhanced by 54.71% at 1.5 LPM and radiation intensity of 800 W/m²K. Comparative analysis of MWCNT and paint, graphene, and paint, and MWCNT and graphene blended paint polymer has been carried out, from which it can be easily seen that all nano-blended polymer gives better thermal performance enhancement when used as collector polymers in FPSC.

Acknowledgments

The authors affirm that they hold no financial interests or personal associations that could have influenced the work reported in this study.

NOMENCLATURE

EDAX: - "Energy dispersive X-ray analysis"
FESEM:- "Field emission scanning electron microscope"
FPSC:- "Flat plate solar collectors"

MWCNT: - "Multi-Wall Carbon Nanotubes"
XRD: - "X-ray diffraction"

Subscripts

A_c: Collector surface area
C_p: Fluid's specific heat capacity
FR: Heat removal efficiency factor
Q: Total energy incident on the solar collector
Q_u: Net heat energy absorbed by the fluid
T_{ab}: Ambient (surrounding) temperature
T_{in}: Fluid temperature at the inlet
T_{out}: Fluid temperature at the outlet

Symbols

V: Rate of volumetric flow
T: Temperature level
K: Heat conductivity coefficient
m: Rate of mass flow

Greek Symbols

β (beta): Tilt angle of the collector
η (eta): Instantaneous thermal efficiency
η_{FPC}: Efficiency of the flat plate collector
$\eta_{Siu.}$: Correlation-based efficiency
$\eta_{exp.}$: Experimentally measured efficiency

REFERENCES

1. Palaniappan M, Palanisamy S, Khan R, Alrasheedi NH, Tadepalli S, Mani T, et al. Synthesis and suitability characterization of microcrystalline cellulose from *Citrus × sinensis* sweet orange peel fruit waste-based biomass for polymer composite applications. J Polym Res. 2024;31.
2. Tyagi A, Vats P, Nair R, Das SK, Bhandari M, Meena A. Experimental investigation of micro-hardness and tribological behavior of composite coating for wear resistance application. J Polym Compos.
3. Juliyana SJ, Prakash JU, Rubi C, Kumar K, Subramaniyam A, Whitin P. Drilling parameters optimization in LM6/B_4C/fly ash hybrid composites by Taguchi technique. 2025.
4. Anand A, Tiwari SK, Prakash V, Gautam SK, Singh RK, Kaushik K. Influence of TiB_2 wt.% on the microstructural and mechanical properties of in-situ processed stir-cast metal matrix composite of Al-6061. J Polym Compos. 2025;13:655–661.
5. Mahawar P, Sharma P, Kumar SJ. Vibration characteristics of copper–aluminum composite. J Polym Compos. 2025;13(Spec Iss 1):190–203.
6. Ali MF, Pasha SA, Hussaini SM. Wear attribute of aluminum metal matrix composite reinforced with MWCNT, produced by FSP, on a vertical milling machine. J Polym Compos. 2025;13(Spec Iss 1):525–539.
7. Chaudhary R, Kumar V, Kumar A, Gupta S, Vivek K. Water hyacinth-derived biopolymers as reinforcements for sustainable fiber-reinforced polymer composites. J Polym Compos. 2025;(Spec Iss 1):1012–1017.
8. Alvarez DL, Al-Sumaiti AS, Rivera SR. Estimation of an optimal PV panel cleaning strategy based on both annual radiation profile and module degradation. IEEE Access. 2020;8:63832–63839.
9. Ajith Arul Daniel S, Pugazhenthi R, Kumar R, Vijayananth S. Multi-objective prediction and optimization of control parameters in the milling of aluminum hybrid metal matrix composites using ANN and Taguchi–grey relational analysis. Def Technol. 2019.
10. Murugan M, Saravanan A, Elumalai P, Kumar P, Saleel CA, Samuel OD, et al. An overview on energy and exergy analysis of solar thermal collectors with passive performance enhancers. Energy. 2022;61(10):8123–8147.

11. Dev R, Kashyap Y, Tewari K, Pal P. Solar distillation and water heating systems integration with photovoltaic technology. In: Renewable Energy: Accelerating the Energy Transition. 1st ed. Berlin: Springer; 2023. p. 139–165.
12. Allouhi A. A novel grid-connected solar PV-thermal/wind integrated system for simultaneous electricity and heat generation in single family buildings. J Clean Prod. 2021;320:128518.
13. Diez F, Navas-Gracia L, Martinez-Rodriguez A, Correa-Guimaraes A, Chico-Santamarta L. Modeling of a flat-plate solar collector using artificial neural networks for different working fluid flow rates. Sol Energy. 2019;188:1320–1331.
14. Gunn A, Jerolmack DJ. Conditions for aeolian transport in the solar system. Nat Astron. 2022;6(8):923–929.
15. Shiraishi Y, Jio M, Yoshida K, Nishiyama Y, Ichikawa S, Tanaka S, et al. Nafion-integrated resorcinol–formaldehyde resin photocatalysts for solar hydrogen peroxide production. ACS Catal. 2023;3(8):2237–2246.
16. Sigalotti LDG, Cruz FJ. Unveiling the mystery of solar-coronal heating. Phys Today. 2023;76(4):34–40.
17. Sözen A, Menlik T, Ünvar S. Determination of efficiency of flat-plate solar collectors using neural network approach. Expert Syst Appl. 2008;35(4):1533–1539.
18. Maldonado-Salguero P, Bueso-Sanchez MC, Molina-Garcia A, Sanchez-Lozano JM. Spatio-temporal dynamic clustering modeling for solar irradiance resource assessment. Renew Energy. 2022;200:344–359.
19. Mansour RB, Khan MAM, Alsulaiman FA. Optimizing the solar PV tilt angle to maximize the power output: A case study for Saudi Arabia. IEEE Access. 2021;9:15914–15928.
20. Colangelo G, Milanese M. Numerical simulation of thermal efficiency of an innovative Al_2O_3 nanofluid solar thermal collector: Influence of nanoparticles concentration. Therm Sci. 2017;21(6 Pt B):2769–2779.
21. Lv J, Xie J, Mohamed AGA, Zhang X, Feng Y, Jiao L, et al. Solar utilization beyond photosynthesis. Nat Rev Chem. 2023;7(2):91–105.
22. Visa I, Moldovan M, Duta A. Novel triangle flat plate solar thermal collector for facades integration. Renew Energy. 2019;143:252–262.
23. Nikolic NN, Lukic NS, Nesovic AM, Nikolic DM. Optimal size and position of the planar back reflector moveable only in the direction normal to the bifacial solar collector plane. Therm Sci. 2024.
24. Martinez-Sanchez RA, Rodriguez-Resendiz J, Alvarez-Alvarado JM, Macias-Socarras I. Solar energy-based future perspective for organic Rankine cycle applications. Machines. 2022;13(6):944.
25. Hussain MM, Concetti C, et al. “Here comes the sun”: Determinants of solar farm planning at local level in England. Energy Policy. 2025;120:103916.
26. Balaji S. γ-Ray and ultra-high energy neutrino background suppression due to solar radiation. Phys Lett B. 2023;845:138157.
27. Simoes S, Simoes T, Barbosa J, Rodrigues C, Azevedo P, Cardoso JP, et al. Estimativa de potenciais tecnicos de energia renovavel em Portugal: eolico, solar fotovoltaico, solar concentrado, biomassa e oceanos. 2023.
28. Bindra A, Gajanana S, Kumar D. Microstructural characterization and analysis of mechanical behavior of hybrid AA7075/7178 fabricated using die casting technique. J Polym Compos. 2025;13(Spec Iss 1):441–451.
29. Hasanzaeh M, Kamran KV, Feizizadeh B, Mollabashi SH. GIS-based spatial decision-making approach for solar energy site selection, Ardabil, Iran. Int J Environ Geosci. 2024;9(1):115–130.
30. Saedodin S, Zaboli M, Ajarostaghi SSM. Hydrothermal analysis of heat transfer and thermal performance characteristics in a parabolic trough solar collector with turbulence-inducing elements. J Sol Energy Eng. 2021;46:101266.
31. Radonjic I, Pavlovic T, Mirjanic D, Pantic L. Investigation of fly ash soiling effects on solar modules performances. Sol Energy. 2021;220:144–151.

32. Padmanabhan RG, Rajesh S, Karthikeyan S, Palanisamy S, Ilyas RA, Ayrilmis N, et al. Evaluation of mechanical properties and Fick's diffusion behavior of aluminum–DMEM reinforced with hemp/bamboo/basalt woven fiber metal laminates under different stacking sequences. Ain Shams Eng J. 2024;15(7):102759.
33. Surendernath P, Pothamsetty Kasi VRMVSK. Evaluation of impact strength and hardness for polymer matrix composites with steel, carbon, and glass reinforcements for automotive applications. J Polym Compos. 2025;13(Spec Iss 1):738–748.
34. Palanisamy S, Mayandi K, Azeez A, Palaniappan M, Rajini N, Santulli C. Wear properties and post-moisture absorption mechanical behavior of kenaf/banana-fiber-reinforced epoxy composites. Fibers. 2022;10:32.
35. Verma SK, Sharma K, Gupta NK, Soni P, Upadhyay N. Performance comparison of innovative spiral-shaped solar collector design with conventional flat plate solar collector. Energy. 2020;194:116853.
36. Mondal R, Ghanta R, Shukla M, Tanmay C. Synthesis of magnetically recoverable nickel(II) complex-functionalized Fe_3O_4@ISNA nanomaterials: Catalytic studies on nitrophenol reduction and TD-DFT studies. J Polym Compos**.** 2024;13(Spec Iss 1).
37. Sharma R, Sharma K, Saraswat BK. Machining process parameters optimization of aluminum alloy AA6262-T6 for CNC turning by grey relational analysis**.** IOP Conf Ser Mater Sci Eng. 2021;1116(1):012016.
38. Almeshaal M, Palanisamy S, Murugesan T, Palaniappan M, Santulli C. Physico-chemical characterization of *Grewia monticola* Sond fibers for prospective application in biocomposites. J Nat Fibers. 2022;19:1–15.
39. Sharma R, Sharma K, Singh D, Mausam K, Singh RP, editors. Investigation of optimum process parameter on CNC turning for aluminum alloy AA6262 using grey relational analysis. Singapore: Springer; 2021.
40. Kumar D, Barthwal S, Praveen P. An overview of the impact of reinforcement on mechanical and thermal characteristics of aluminum alloy composites. J Polym Compos**.** 2025;13(Spec Iss 1):240–249.
41. Mausam K, Gola V, Ghosh S. FPC thermal performance enhancement and reduction of greenhouse gas emissions: A sustainable approach using nanoparticles**.** Mater Today Proc**.** 2023.
42. Tyagi A, Vats P, Nair R, Das SK, Shahid M, Amit M. Experimental analysis of residual stress, micro-hardness and corrosion behavior of HVOF sprayed composite coating. J Polym Compos. 2025;13(Spec Iss 1):77–82.
43. Goutham E, Hussain S, Muthukumar C, Krishnasamy S, Thiagamani SMK, Santulli C, et al. Drilling parameters and post-drilling residual tensile properties of natural-fiber-reinforced composites: A review**.** J Compos Sci**.** 2023;7:136.
44. Mausam K, Singh S, Ghosh S, Singh RP, Tiwari A. Experimental analysis of the thermal performance of traditional parallel tube collector and cutting-edge spiral tube collector: A comparative study. Therm Sci Eng Prog**.** 2024;47:102295.
45. Klein SA. Calculation of flat-plate solar collector loss coefficients. Sol Energy. 1979;17(1):79–80.
46. Duffie JA, Beckman WA. *Solar Engineering of Thermal Processes*. 3rd ed. New York: Wiley; 2006. p. 1–900.
47. Dasaien AV, Elumalai N. Performance enhancement studies in a thermosyphon flat plate solar water heater with CuO nanofluid. Therm Sci**.** 2017;21(6 Pt B):2757–2768.

